

# ACTIVATION OF FIELD EMITTERS ON CLEAN NIOBIUM SURFACES

A. Navitski, S. Lagotzky, G. Müller, FB C Physics, University of Wuppertal, 42097, Germany

D. Reschke, X. Singer, DESY, 22603 Hamburg, Germany

## Abstract

Systematic investigations of the influence of heat treatments of high-purity Nb samples at temperatures between 122°C and 800°C on the parasitic field emission are reported. Two large grain and two single crystal Nb samples were used. The samples got up to 40µm final BCP polishing and high pressure ultra pure water rinsing at DESY. The heat treatment of the Nb samples has led to a definite activation of field emitters on the surface. The emitter number density increases significantly with temperature of the heat treatment.

## INTRODUCTION

Heat treatments (HT) of superconducting Nb cavities have become a very important part of the preparation procedure for hydrogen degassing after electropolishing of the cavities [1]. Furthermore, a bakeout at temperature between 100°C and 170°C for 48 hours improves the quality factor  $Q_0$  of cavities at high gradients. This effect is confirmed for cavities that got buffered chemical polishing (BCP) as well as for electropolished (EP) ones before the final high pressure rinsing (HPR) with ultra pure water [2-3]. The improvement of  $Q_0$  is explained by the diffusion of oxygen away from the oxide layer at the surface into the superconducting Nb bulk. Thereby the surface resistance  $R_s$  decreases and the critical field increases [2, 4]. The cavity preparation for the European XFEL contains two bakeouts: early at 800°C after the initial polishing and finally at 120°C just before the vertical test [5].

Former results have shown that annealing of the Nb surface at temperatures of 400 to 800°C can activate field emission (FE) at electric onset field  $E_{on}$  (required for 1 nA FE current) down to 40 MV/m [6]. Experiments with large grain Nb samples have also shown a grain boundary assisted FE at about 200 MV/m after a bakeout at 150°C for 14 hours [7]. Since FE is one of the main field limitations of the high gradient superconducting cavities required for XFEL and ILC, we have systematically investigated the influence of such different HT on the FE behaviour of single crystal (SC) and large grain (LG) Nb samples prepared at DESY.

## EXPERIMENTAL TECHNIQUES

For the systematic investigations of parasitic FE from the Nb samples we have used a specially constructed non-commercial field emission scanning microscope (FESM) shown in Fig. 1 [8]. The FESM is an advanced microscope for investigation of FE site distributions on

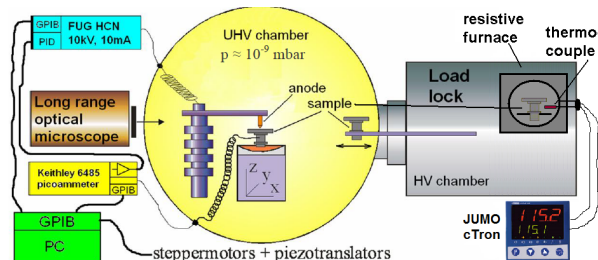


Figure 1: Schematic view of the FESM microscope.

“flat” cathodes of up to 25 x 25 mm<sup>2</sup>. The cathode is xy-surface tilt-corrected with respect to the anode to achieve a constant gap  $\Delta z$  within  $\pm 5 \mu\text{m}$  for the full scan area. The measurements are done in ultrahigh vacuum (UHV) of  $10^{-9}$  mbar by means of non-destructive regulated voltage scans  $V(x, y)$  at a fixed FE current (typ. 1 nA). It employs a PID-regulated power supply FUG HCN100M-10000 controlled by the FE current as measured with a digital picoammeter Keithley 6485 or an analog electrometer Keithley 610C described elsewhere [9]. The power supply provides up to 10 mA current and 10 kV voltage, which corresponds to 500 MV/m macroscopic field at 20  $\mu\text{m}$  gap. By in-situ exchange between needle-anodes and truncated cone anodes, the emitter distribution and emitter number density on selected areas of the samples can be verified with the required resolution. The activation field  $E_{act}$ , onset field  $E_{on}$  as well as field enhancement factor  $\beta$  and emitting area  $S$  of arbitrarily chosen individual emitters can be measured as well. The last two parameters are calculated from the measured I-V characteristics of the emitters using the modified Fowler-Nordheim law [10] for field emission:

$$I_{FN} = A \frac{SE^2}{\phi t^2(y)} \exp\left(-B \frac{\phi^{3/2} \nu(y)}{E}\right)$$

The needle anodes have a tip apex radius of  $R_a \geq 1 \mu\text{m}$ , while the truncated cone anodes are up to 300  $\mu\text{m}$  in diameter. The macroscopic electric field  $E$  is calibrated for each emitter as the linear slope of the PID-regulated  $V(z)$  dependence for 1 nA current. Moreover, the real distance  $d$  between the tip anode and the relevant emitter is determined by the linear extrapolation of each  $V(z)$  curve to zero voltage [11].

The load lock (preparation) chamber of the FESM was recently equipped with a resistive furnace which is used for the annealing of samples up to 1200°C under HV conditions ( $< 10^{-6}$  mbar). The temperature inside the

furnace is measured with a thermocouple (Pt10Rh-Pt S) and is controlled by a commercial PID-controller (JUMO cTRON 04). The samples are transported inside the system by means of several mechanical translators and are always at least under HV conditions during measurement sequences. Transport of the samples to external setups (OP, FESM, and SEM) are always done under protection caps (see Fig. 4) and sealed in plastic bags to avoid any contaminations as much as possible.

The FESM investigations of HT effects were done sequentially in four steps. As first step, the FE of the initial BCP/HPR treated surface was measured. The other

Table 1: Parameters for the different HTs

	Temperature, °C	Duration, h	Warm-up, °C/min
HT122	122	24	~0.54 (3h)
HT400	400	2	~6.25 (1h)
HT800	800	2	~12.91 (1h)

three steps followed after different HTs: HT122, HT400, HT800. An overview of the HTs is given in Table 1.

Each FE investigation is done by means of the voltage scans (using  $\varnothing = 300 \mu\text{m}$  anodes,  $50 \mu\text{m}$  gap at fixed FE current of 1 nA) in the same area with sequential field increase between 100 and 160 MV/m in 20 MV/m steps. A region of  $1 \text{ cm}^2$  was scanned with  $67 \times 67$  points (lateral resolution around  $150 \mu\text{m}$ ). The HTs consist of three stages: a warm-up stage where the sample is heated up from room to the desired temperature, a heat treatment at constant temperature ( $\pm 1^\circ\text{C}$  fluctuations), and a cool-down stage after turning off the furnace. The cool-down stage takes usually several hours depending on the HT temperature. An example of the temperature ramp for

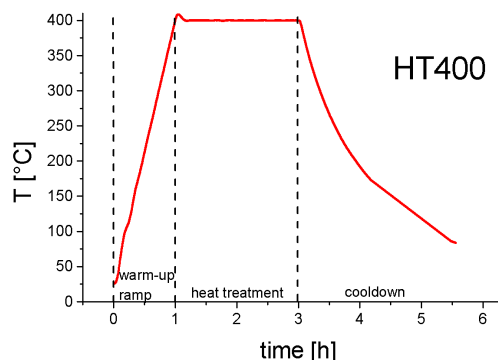


Figure 2: An example of temperature ramp as for HT 400 with the three different stages.

HT400 is shown in Fig. 2. There was observed typically some pressure increase in the vacuum chamber, especially for the HT800, but it never exceeded  $10^{-6}$  mbar.

The surface quality and defects on the samples are examined by means of optical profilometer (OP) with atomic force microscope (AFM) and scanning electron microscope (SEM) with energy dispersive x-ray analysis



Figure 3: Optical profilometer with AFM.

(EDX). The OP with AFM is a commercial apparatus (FRT GmbH) and is shown in Fig. 3. It is installed on a massive granite plate with an active vibration damping system. The system contains a horizontal laminar air flow from the back (class 5 ISO) for cleanroom-like conditions. The profilometer measurement setup contains a CCD camera for fast positioning, the OP based on a spectral reflection (chromatic aberration) of white light and the AFM in calibrated positions ( $2 \mu\text{m}$  positioning accuracy with respect to the OP). Samples of up to  $20 \times 20 \text{ cm}^2$  and 5 cm height difference can be measured non-destructively with a maximal lateral (vertical) resolution of  $2 \mu\text{m}$  ( $3 \text{ nm}$ ) in case of OP. Further zooming down to the nm range is possible with the AFM for a maximum area of  $80 \times 80 \mu\text{m}^2$  in contact or non-contact modes.

The OP measurements of the samples have been performed in two steps. At first full scans of the sample ( $28 \times 28 \text{ mm}^2$ ) with a lateral resolution of at least  $28 \mu\text{m}$  were made to localize the major defects with respect to the marks at the circumference as shown in Fig. 5. Then selected regions of  $1 \times 1 \text{ mm}^2$  with obvious defects were measured with the maximal lateral resolution of the OP. In addition, the grain boundaries of the LG samples as well as some random areas without obvious defects were studied to determine the base roughness  $R_a$  and  $R_q$  of the samples. The OP measurements were made before the second step of the BCP and before the HPR.

## SAMPLES FOR THE STUDY

Four special samples were prepared for these studies. The samples are flat with a diameter of 26.5 mm and were machined from the high-purity ( $\text{RRR} > 250$ ) SC or LG Nb sheets and welded to support rods (Fig. 4). Similar but polycrystalline Nb samples were used for the quality control of chemical treatments of the cavities [12]. There



Figure 4: LG Nb sample with the protection cap.

the samples were assembled in the main coupler port of nine-cell cavities during the wet chemical treatments. In contrast, a simple cavity was used for the BCP of the actual samples. Two special marks on the circumference served to re-identify their angular position during the surface studies. The LG samples contain three large grains with a grain boundary junction in the middle of the sample. The samples got BCP up to 40  $\mu\text{m}$  in two steps: first up to 30  $\mu\text{m}$  and afterwards up to 10  $\mu\text{m}$  to refresh the surface after some waiting time. After the BCP, the samples got high-pressure water rinsing (HPR) at DESY with ultra pure water under clean room conditions and were always transported under the protection cap to avoid pollution. The caps were removed for the first time in the FESM under the base pressure of  $10^{-7}$  mbar.

## RESULTS AND DISCUSSION

### OP Results

The samples were investigated by OP before the second BCP (10 $\mu\text{m}$ ) and showed some defects like scratches or small pits with mostly low  $\beta$  values in the range of 2 to 4. Very few defects showed higher  $\beta_{max}$  up to 13. The typical roughness of the samples was in the range of 50-300 nm ( $R_a$ ) and 70-400 nm ( $R_q$ ). The sample flatness is  $\pm 2 \mu\text{m}$  within the area of 1cm<sup>2</sup> used for the FESM investigations. An example of the surface profiles is shown in Fig. 5.

### FESM+HT Results

The sequential FESM-HT-FESM investigations show a clear increase of emitter number density with increasing of temperature of the HT. It means that the temperature treatment of Nb definitely leads to an activation of new emitters on the surface. Figure 6 shows the sequential field maps measured up to 160 MV/m with the LG sample at the initial state and after each HT. It shows clear activation of emitter by the temperature treatments. The number density of emitters increases significantly with the temperature (Fig. 7). One can see a rise of the emitter number density with the activation field after the different HTs. While it seems to be linear for the HT800, it might be exponential especially for the HT400 case. Similar

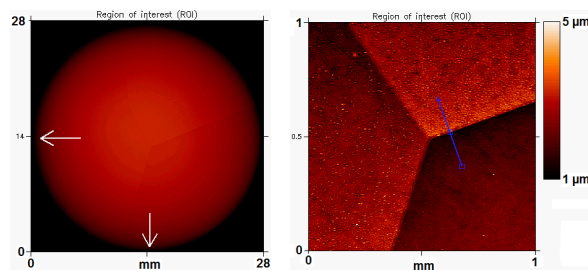


Figure 5: OP profiles of the whole LG Nb sample (left, 28  $\mu\text{m}$  lateral resolution, the arrows indicate the marks) and the grain junction (right) in the middle of it.

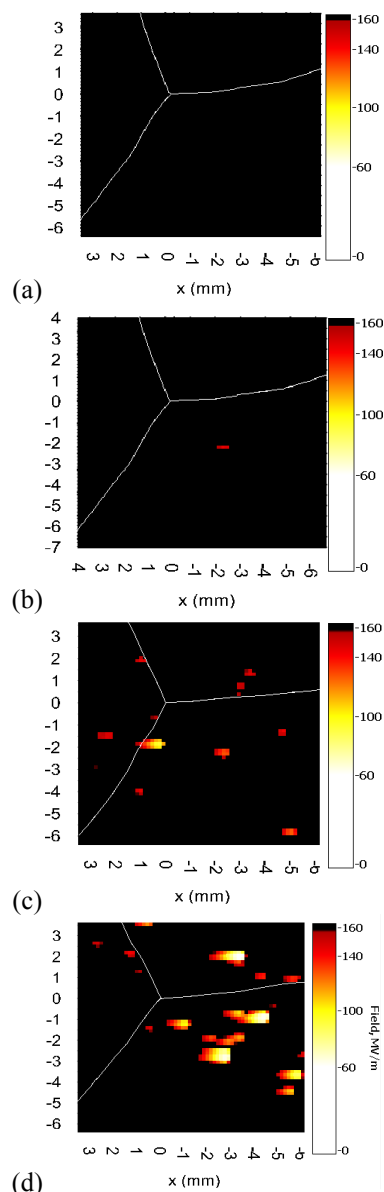


Figure 6: Field maps up to 160 MV/m of the LG Nb sample in the same area before the HT (a), after HT122 (b), HT400 (c), and HT800 (d).

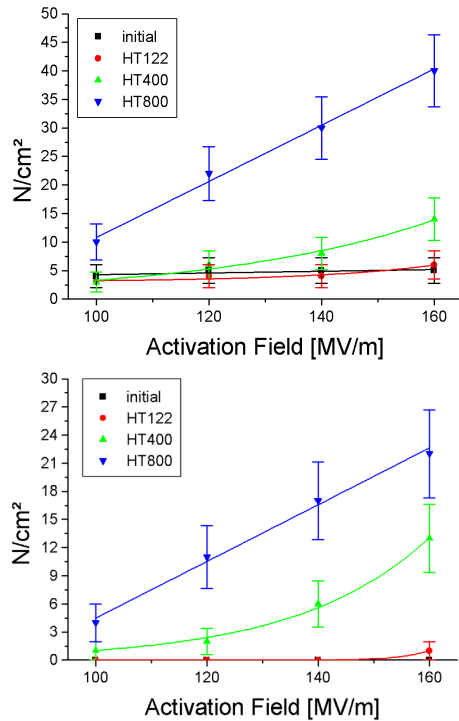


Figure 7: Increase of emitter number density on SC (upper) and LG (lower) Nb samples with increasing of temperature of HT and the activation field.

increase of emitter number density was observed for electropolished polycrystalline Nb samples [9, 13].

On the other side there is activation of emitters due to the electric field, too. Finally the emitters appear at lower onset field (Fig. 8) compared to the initial activation field, i.e. reduced by the field reduction factor  $\rho = E_{act}/E_{on}$ . Therefore, the emitters can be activated either by electric field or by temperature. One can see that most emitters produced by HT are emitting at  $E_{on}$  in the range of 100-

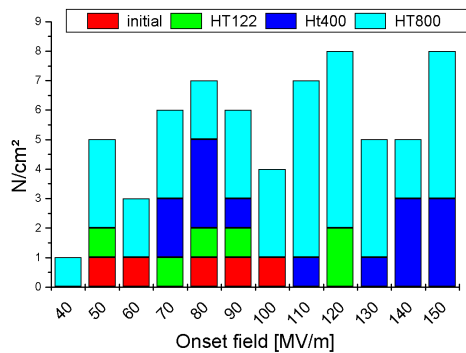


Figure 8: Stacked histogram of the distribution of the onset field  $E_{on}$  after each HT.

160 MV/m, but some already at 40 MV/m surface field, what is already most relevant for the XFEL machines.

It was interesting to compare the  $\rho$  values and the ratio of emitters activated by field ( $N_{act}^E/N$ ) and by

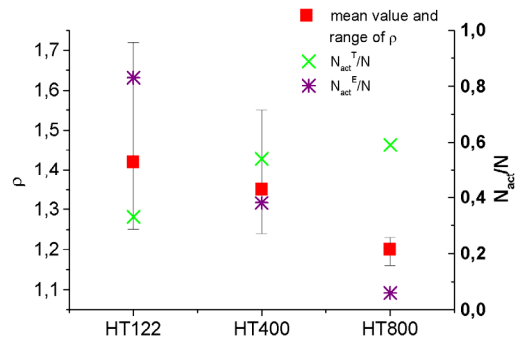


Figure 9: The field reduction factor  $\rho$  (left y axis) and the ratio of field activated and HT activated emitters (right y axis).

temperature ( $N_{act}^T/N$ ). In Fig. 9 one can see that  $\rho$  lies in the range of 1.2 to 1.4 and becomes smaller for higher temperature of HT. This is expected since the activation by temperature should be a slow process compared to the activation by field. In case of polycrystalline Nb samples the field reduction factors were in the range of 2-4 (without any HT) [9, 13]. It means the oxide thickness and crystal structure influence the field activation of emitters. The surface oxide seems to be responsible for the activation effect. Roughening the surface due to an oxygen redistribution and breakdown of the surface oxide are probably the main effects leading to the activation of the parasitic emission.

Comparing the ratios of field- and temperature-activated emitter it is obvious that there is a number of potential placed which can be activated as field emitters of the surface. In our case it happens due to dc electric field or temperature. It is challenging to find out if the rf power in the cavities can lead to an immediate activation of FE from the potential places. The grain boundary assisted FE [7] could yet not be confirmed for the actual BCP/HPR treated LG Nb samples.

### CONCLUSION AND OUTLOOK

The HT of LG and SC Nb samples definitely lead to activation of field emitters. A significantly increase of the emitter number density with temperature can be observed. Emitter activation occurs either by field or temperature: the ratio of T-activated emitters raises with temperature of HT, while that of the E-activated emitters decreases. It means there are a number of potential spots on the Nb surface which can become field emitters in different ways. A possible activation of such emitters due to the rf power is a challenging question. The surface oxide seems to be responsible for the activation effect. The oxide thickness and crystal structure influence the field activation of emitters.

Local FE measurements of single emitters for  $\beta$  and  $S$  determination as well as their correlation to SEM/EDX and Auger investigations will follow to reveal the nature of the field emitters. Furthermore, measurements of the

oxide layer thickness after each HT is to be done to understand its possible role in the emitter activation.

### ACKNOWLEDGMENTS

Acknowledgements are given to Dr. R. Heiderhoff for access to SEM facility at FB E of University of Wuppertal and to J. Ziegler for a help with HPR treatment at DESY. The work is funded by Helmholtz-Allianz "Physics at the Terascale" and BMBF project O5H09PX5.

### REFERENCES

- [1] H. Padamsee, RF Superconductivity, WILEY-VCH (2008).
- [2] B. Visentin et al., "Improvements of Superconducting Cavity Performances at High Accelerating Gradients", Proc. of the 6<sup>th</sup> EPAC, Vol. III p.1885, Stockholm SWEDEN (1998).
- [3] B.Visentin, J.P.Charrier, B.Coadou, D.Roudier, Proc. of 9<sup>th</sup> SRF-Workshop, Los Alamos, p. 198 (1999).
- [4] G. Ciovati, "Improved oxygen diffusion model to explain the effect of low-temperature baking on high field losses in niobium superconducting cavities", Appl. Phys. Letters 89, 022507 (2006).
- [5] D. Reschke et al.; Phys. Rev. ST – Accel. Beams 13, 07100-1 (2010).
- [6] E. Mahner SRF1993.
- [7] A. Dangwal, G.Müller, D.Reschke, X.Singer, Phys. Rev. ST – Accel. Beams 12, 023501-1 (2009).
- [8] D. Lysenkov and G. Müller, Int. J. Nanotechnol. 2, 239 (2005).
- [9] A. Navitski, PhD thesis, Univ. of Wuppertal, 2010
- [10] R. G. Forbes, J. Vac. Sci. Technol. B 17, 526 (1999).
- [11] A. Navitski, G. Müller, V. Sakharuk, T.W. Cornelius, C. Trautmann, and S. Karim, Eur. Phys. J. Appl. Phys. 48, 30502 (2009).
- [12] G. Müller, A. Göhl, T. Habermann, A. Matheisen, D. Nau, D. Proch, and D. Reschke, Proc. of 6th Eur. Part. Acc. Conf. EPAC 98, Stockholm, p. 1876 (1998).
- [13] 4<sup>th</sup> annual workshop of the Helmholtz Alliance "Physics at the Terascale", Dresden, 2010.